Environ Fluid Mech (2017) 17:395–413
DOI 10.1007/s10652-016-9497-5

ORIGINAL ARTICLE

Application of CFD modelling to air quality in Kuwait City

Meruyert Zhunussova[1] · **Martin Jaeger**[2] · **Desmond Adair**[3]

Received: 1 June 2016 / Accepted: 21 November 2016 / Published online: 30 November 2016

Abstract High-resolution computational fluid dynamics (CFD) simulations have been performed to assess the dispersion of air pollutants (CO_2) emanating from traffic in a busy street and in the vicinity of a complex configuration of buildings located in Salmiya, Kuwait City. New buildings are planned for this area, and the work here includes predictions for the dispersion of pollutants after the buildings' completion. The CFD simulations are based on calculated CO_2 concentration levels for traffic counts taken on location in Salmiya with the existing configuration of buildings. As the computer code used in this work has been evaluated previously, it will be applied here to predict with confidence any potential air pollution problem areas on the addition of the new buildings. It was found for very light wind, that the proposed new buildings help reduce pollution in the vicinity of residential buildings within the configuration of buildings, but as the wind becomes moderate to strong, there was a tendency for the pollutant to get trapped in the residential area. Results are given for both exceptionally high ambient temperatures and very light wind, which are not often reported in studies found in the literature.

Keywords Computational fluid dynamics (CFD) · Built environment · Street canyon · Air quality · Light wind

1 Introduction

Within the last years, micro-scale computational fluid dynamics (CFD) models have become an efficient and common simulation tool for assessment and prediction of air quality in urban areas. The urban environment, from the point of view of air pollution, is

✉ Martin Jaeger
M.Jaeger@ack.edu.kw

[1] Department of Civil Engineering, Nazarbayev University, Astana 010000, Republic of Kazakhstan

[2] Department of Civil Engineering, Australian College of Kuwait, Mishref, Kuwait

[3] Department of Mechanical Engineering, Nazarbayev University, Astana 010000, Republic of Kazakhstan

gradually becoming more complex, and increasing density of traffic leads to much greater traffic emissions and hence greater air pollution, especially where buildings form a complex configuration of street canyons. Transport vehicles are by far the major emission source of nitrogen oxides and hydrocarbons in urban areas [1, 2]. Vehicular exhausts dominate air pollution in cities because traffic in these cities is usually dense and engines often run cold and at idle [3]. Despite significant improvements in fuel and engine technology [4, 5] it is now generally recognized that many of the substances directly emitted by vehicles into the ambient air, or, indirectly produced through photochemical reactions, represent a serious hazard for human health [6, 7]. The main traffic-related pollutants are CO, CO_2, NO_x, hydrocarbons, and particles. CO is an imperfect fuel combustion product. Combustion also produces a mixture of NO_2 and NO, of which more than 90% is in the form of NO.

Considerable resources are devoted in more advanced countries to the measurements of air pollutant concentrations at discrete points in the built environment. However, these measurements on their own do not cover entire urban areas satisfactorily nor give much evidence of how air pollution is actually dispersed. Therefore, neither the impact on human health nor the adequacy of control measures has been properly quantified. Also, there is a frequent need for detailed knowledge of the dispersion characteristics of pollutants emitted to the atmosphere and the environmental impact assessment of new developments within city centres, including their impact on the concentration of air pollutants within microenvironments [8]. This paper is showing how to meet this need.

Gradually the well-held view that CFD modelling is very complicated is being overcome and its advantages to predict concentration fields near complex buildings better regarded. Many works can be found in the literature reporting on the use of CFD techniques to model flow and pollutant dispersion around isolated buildings or groups of buildings [9–13]. Flow and pollutant dispersion from street-scale to neighbourhood-scale have been widely investigated, often coupling wind tunnel/field experiments with CFD simulations [14–16]. Recently, several works have provided in-depth reviews of the state of both dispersion physics and computational wind engineering [17, 18]. The Reynolds-averaged Navier–Stokes equation (RANS) methods are amongst the most preferable procedures used to model urban dispersion problems, mainly due to their relatively inexpensive computational costs.

In this work such a model is used to assess the dispersion of air pollutants (CO_2) emanating from traffic in a busy inner-city street and in the vicinity of a complex configuration of buildings located in Salmiya, Kuwait City. New buildings are planned for this area, and the work here includes predictions for the dispersion of pollutants on their addition. The dispersion process is driven by onset wind flow and buoyancy, and, the CFD simulations are performed with 3D RANS equations and the Renormalization Group (RNG) k–ε turbulence model [19] to model the turbulence. This turbulence model has already been proved suitable for modelling air pollution at the local urban scale [20] and the CFD model as a whole has the potential for providing regulatory evidence. As Kuwait City exists in a particularly hot climate, with at times very light winds, the model used here included buoyancy. Several recent publications [21, 22] include comprehensive and useful details to what should be generally included when buoyancy and stratification need to be considered. The CFD model has been used to predict wind characteristics for a simple boundary-layer flow over a rough surface, concentrations of pollutants (C_2H_6, NO_x) for a two-dimensional street canyon, and, characteristics of the flow and concentration levels (CO, CO_2) over a geometrically more complicated three-dimensional urban environment [23, 24]. The calculations give interesting results for different onset wind conditions and

provide evidence on how dispersion of pollutants can be predicted after the built environment has been altered.

2 Description of urban environment and measurements

A schematic of the urban environment used in this study is shown on Fig. 1. The pollutants emanating from traffic on Salem Mubarak Street (running in SWW direction, between Buildings 11 and 12 on one side, and the proposed new Buildings 13 and 14 on the other side) affects the air quality in the proximity of the residential high rise buildings SE of the new proposed Building 13 (i.e. residential Buildings 2–9). Although there is also pollutants emitted from vehicles travelling along the other roads shown on Fig. 1, for this study we are interested in the prevailing wind during winter and summer (i.e. NW), which constitutes the 'worst case' scenario for pollution problems in the vicinity of the considered residential buildings. Since high temperatures during summer add to a negative impact on health, wind from the NW, and, with an ambient temperature of 50°C, are considered. An average ambient temperature of 25 °C is set for the winter conditions.

Only traffic travelling along Salem Mubarak Street within the investigated section (240 m, between existing Building 11 and proposed new Building 13) will be used as a line source of pollutant. Traffic through this street is characterized by frequent traffic interruptions by traffic participants who seek to park or leave the parking position of their vehicle on the lateral parking area (lateral parking lots in both directions). Because of the predominant low vehicle speed, turbulence induced by moving vehicles was ignored.

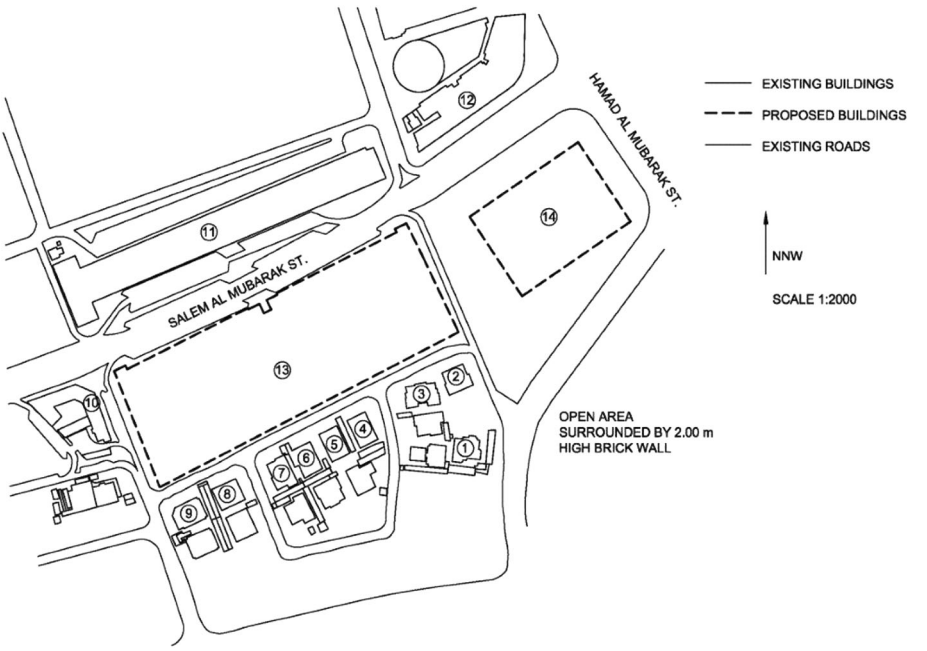

Fig. 1 A schematic of the urban environment used in this study

The approximate geometric characteristics of the considered buildings are shown in Table 1.

The proposed commercial complexes, Buildings 13 and 14, are part of a new mall which is currently under construction. Although the usage as a shopping centre will most likely lead to an increase in traffic volume, for the purpose of this study (i.e. impact of new buildings on air quality) the same traffic volumes of the pre-construction situation will be used for the post-completion situation.

Weekly traffic volumes of traffic passing through the investigated corridor and recorded for 24 h per day, was received from the local traffic department. Based on this data, which was confirmed by manual on-spot counts on three different weekdays, the average weekday Morning peak volume of 426 vehicles per hour was identified as the highest traffic volume of the investigated corridor (Table 2) [25].

The total amount of CO_2 emission depends on the fuel consumption which is a function of the vehicle velocity and vehicle model. For the situation here, the average vehicle velocity was found to be 14 km/h with an average fuel consumption of 25 l/100 km [25]. This leads to a total fuel consumption within the investigation section of,

$$426\left(\frac{\mathrm{V}}{\mathrm{h}}\right) \times 25\left(\frac{1}{\mathrm{V} \times 100\,\mathrm{km}}\right) = 25.56\left(\frac{\mathrm{l}}{\mathrm{h}}\right).$$

The CO_2 emissions for the investigation segment considered here (length = 240 m) can be determined based on the observation of 95% light/medium vehicles (i.e. gasoline powered vehicles), 0.64 kg gasoline carbon content per liter, 99% oxidation factor of carbon content in gasoline and a molecular weight of CO_2 to C ratio of 44/12,

$$\begin{aligned} \mathrm{CO}_{2,\mathrm{gas}} &= 25.56\left(\frac{\mathrm{l}}{\mathrm{h}}\right) \times 0.95\left(\frac{\text{Passenger vehicles}}{\text{Total vehicles}}\right) \times 0.64\left(\frac{\mathrm{kg}}{\mathrm{l}}\right) \times \frac{99}{100} \times \frac{44}{12} \\ &= 56.334\left(\frac{\mathrm{kg}}{\mathrm{h}}\right) = 15.64\left(\frac{\mathrm{g}}{\mathrm{s}}\right) = > \frac{15.64}{240} = 0.065\left(\frac{\mathrm{g}}{\mathrm{ms}}\right). \end{aligned}$$

Table 1 Geometric characteristics of considered buildings (locations shown on Fig. 1)

Building no.	Status	Length	Width	Height (# floors equivalent)[a]
2	Existing, residential	20	20	3
3	Existing, residential	20	20	3
4	Existing, residential	20	20	3
5	Existing, residential	20	20	3
6	Existing, residential	20	20	9
7	Existing, residential	20	20	10
8	Existing, residential	20	20	10
9	Existing, residential	20	20	4
11	Existing, commercial	240	25	4
12	Existing, commercial	100	30	7
13	Proposed, commercial	230	90	8
14	Proposed, commercial	100	70	6

[a] One floor height is equivalent to 4 m

Table 2 Average weekday morning peak volume

Peak	Traffic flow direction	Traffic volume (Vph)
AM	SWW	293
	ENE	133
AM_{tot}	Both	426

This is the mass of CO_2 gas emitted per metre per second from two sources placed in 'Salem Al Mubarak St.' for a length of 240 m. Two horizontal sources were used to simulate the emissions of exhaust gases from vehicles more realistically in the following calculations, as will be described in Sect. 4.

3 CFD methodologies and model description

The air quality model to calculate pollutant levels at the local urban scale was PHOENICS [26] together with some FORTRAN-coding sequences added through user-accessible subroutines, and contains two sub-models: one to calculate the wind velocity and pressure (and if necessary the temperature) characteristics, and the other to calculate concentration diffusion. The wind distribution over the urban region is solved first, with the results used by the concentration diffusion model to obtain the concentration characteristics for the same region. As the velocity of the wind is at low subsonic speeds, the flow is taken to be incompressible. The governing equations of the model are:

Continuity equation

$$\frac{\partial U_j}{\partial x_j} = 0 \tag{1}$$

Momentum equations

$$\frac{\partial U_i}{\partial t} + U_j \frac{\partial U_i}{\partial x_j} = -\frac{1}{\rho}\frac{\partial p}{\partial x_i} + \frac{\mu}{\rho}\frac{\partial^2 U_i}{\partial x_j \partial x_j} - \frac{\partial}{\partial x_j}\left(\overline{u_i u_j}\right) + \delta_{i3} g_i \tag{2}$$

Energy equations

$$\frac{\partial T}{\partial t} + U_j \frac{\partial T}{\partial x_j} = \frac{1}{\rho}\frac{\partial}{\partial x_j}\left[\left(\frac{\mu}{Pr} + \frac{\mu_t}{\sigma_t}\right)\frac{\partial T}{\partial x_j}\right] \tag{3}$$

Species (pollutants) transport equations

$$\frac{\partial C_i}{\partial t} + U_j \frac{\partial C_i}{\partial x_j} = \frac{1}{\rho}\frac{\partial}{\partial x_j}\left[\left(D_i + \frac{\mu_t}{Sc_t}\right)\frac{\partial C_i}{\partial x_j}\right] \tag{4}$$

Transport equations for RNG k–ε turbulence model

$$\frac{\partial k}{\partial t} + U_j \frac{\partial k}{\partial x_j} = \frac{1}{\rho}\frac{\partial}{\partial x_j}\left[\alpha_k \mu_{eff}\frac{\partial k}{\partial x_j}\right] + \frac{G_k}{\rho} + \frac{G_b}{\rho} - \varepsilon \tag{5}$$

$$\frac{\partial \varepsilon}{\partial t} + U_j \frac{\partial \varepsilon}{\partial x_j} = \frac{1}{\rho}\frac{\partial}{\partial x_j}\left[\alpha_\varepsilon \mu_{eff}\frac{\partial \varepsilon}{\partial x_j}\right] + \frac{1}{\rho} C_{1\varepsilon} G_k \frac{\varepsilon}{k} - \left[C_{2\varepsilon} + \frac{C_\mu \rho \eta^3 (1 - \eta/\eta_0)}{1 + \beta\eta^3}\right]\frac{\varepsilon^2}{k}, \tag{6}$$

where

$$u_i u_j = \frac{1}{\rho}\mu_t\left(\frac{\partial U_i}{\partial x_j}+\frac{\partial U_j}{\partial x_i}\right)-\frac{2}{3}k\delta_{ij} \tag{7a}$$

$$G_k = -\rho\overline{u_i u_j}\frac{\partial U_j}{\partial x_i} \tag{7b}$$

$$G_b = -g_i\frac{\mu_t}{\rho\sigma_t}\frac{\partial \rho}{\partial x_i}, \tag{7c}$$

where U_i, U_j are the time-averaged velocity components, $u_i u_j$ are the Reynolds stresses, $\rho C_\mu k^2/\varepsilon$,, μ_t is the turbulent viscosity; μ is the molecular viscosity; g_i is the gravitational body force; G_k is the turbulent kinetic energy production; G_b is the generation of turbulence kinetic energy due to buoyancy; C_i is the chemical species (pollutants) concentration; T is temperature; Pr is the Prandtl number; σ_t is the turbulent Prandtl number (=0.85); D_i is the diffusivity; and, Sc_i is the turbulent Schmidt number. Equation (7c) for the generation of turbulence kinetic energy due to buoyancy was obtained by assuming that air is an ideal gas.

In this study, the Boussinesq approximation was used to treat the variable air density in which the air density is taken as a constant in all terms of the solved equations, except for the buoyancy term in the momentum equation,

$$(\rho-\rho_0)g = -\rho_0\beta(T-T_0)g, \tag{8}$$

where ρ_0 is the referenced density of the air flow, T_0 is the referenced temperature and β is the volumetric expansion coefficient. Equation (8) is obtained by the Boussinesq approximation $\rho_0(1-\beta\Delta T)$ to replace the buoyancy terms (pressure and gravity terms). This approximation is acceptable as long as changes in actual density are small. Specifically, it is valid when $\beta(T-T_0) \ll 1$ and should not be used if the temperature difference in the domain is large, which is not the case in this work.

The turbulent Schmidt number is necessary to solve the species transport equation with RANS and is defined as the ratio of turbulent momentum diffusivity (eddy viscosity) to the turbulent mass diffusivity ($Sc_t = \nu_t/D_t$). The effect of using different Sc_t values when using RANS has already been presented in various previous publications [27–29] and some consensus has been found on the use of a low value of Sc_t as this will try to correct the predicted dilution by reducing diffusion of species upstream of the emission source, whereas downstream of the emission source a low Sc_t value will increase diffusion. This is what would be required to improve agreement with experimental data, but calibration of numerical dispersion simulations using different Sc_t values cannot be generalized because such values are highly case dependent [30]. For this work a value of $Sc_t = 0.3$ was used throughout.

The RNG k–ε turbulence model is based on the RNG theory [19] and has a similar form to the standard k–ε turbulence model [31], but it provides an analytically derived differential formula for determining the effective viscosity and an additional term for the ε equation. For the RNG turbulence model, α_k and α_ε are the effective Prandtl number for k and ε respectively; μ_{eff} is the effective turbulent viscosity; $\eta = Sk/\varepsilon$, S is the scalar measure of the deformation tensor; and, the constants η_0 and β are 4.38 and 0.012, respectively.

The constants for the RNG k–ε turbulence model used in this work are summarized in Table 3.

The requirements set out in three recent guidelines [32–34] were followed in the present work. The governing Eqs. (1–6) were discretized using a finite volume method with all transport equations discretized using a second-order upwind scheme [35]. The SIMPLE algorithm [36] was used to relate the pressure field to the continuity equation where the velocity and pressure fields were calculated separately, with coupling between the respective variables achieved via velocity and pressure corrections. During the calculations, no under-relaxation factors were used except for the pressure term, which was set at 0.7. The maximum residual for each variable was set at 10^{-4} to achieve convergence. Each case was computed on a Dell 5500 Workstation with an Intel Xeon Six Core Processor (2.66 GHz), and calculations lasted between 10 and 30 min depending on grid size and turbulence model used.

The boundary conditions of the pollutant dispersion model in the urban environment are summarised in Table 4.

Cartesian grids were used throughout this work with extensive tests for independence of grid size checked by increasing the grid numbers until further refinement was shown not to be of significance. Close to solid surfaces, the grid was refined using geometric progression with an expansion ratio from the solid surfaces of less than 1.2 and with the cell size adjacent to the solid surface of not more than 0.1 m.

A mixture of pollutant and air was ejected horizontally from two horizontal sources at a constant flow rate. The velocity (or wind) profile in a neutrally stratified atmosphere was calculated through the logarithmic law,

$$u(z) = \frac{u^*}{k} \ln\left(1 + \frac{z}{z_0}\right), \tag{9}$$

where u^* is the friction velocity, k is the von Karman constant, z_0 is the roughness length and z is the height from the surface. The turbulent kinetic energy and dissipation rate profiles were specified as follows,

$$k = \frac{u^{*2}}{\sqrt{C_\mu}}\left(1 - \frac{z}{\delta}\right) \tag{10}$$

$$\varepsilon = \frac{u^{*3}}{\kappa z}\left(1 - \frac{z}{\delta}\right), \tag{11}$$

where δ is the atmospheric boundary layer depth and C_μ is a coefficient used to define the eddy-viscosity in the RNG k–ε turbulence model.

The geometry of the urban environment to be studied was first build within the computational domain boundary shown on Fig. 2. All numbered buildings were included as was an inlet plane whose attributes are described by Eqs. (9–11). An outlet plane was created with pressure used as the boundary conditions. The top and sides of the computational domain were symmetry planes which were impervious but without friction. The ground plane had a logarithmic law-of-the-wall boundary condition, as had the walls and

Table 3 Constants of the RNG k–ε turbulence model used here

Model	$C_{\varepsilon 1}$	$C_{\varepsilon 2}$	C_μ	α_k	α_ε
RNG	1.42	1.68	0.0845	Formula	Formula

Table 4 Boundary conditions

Model	Inflow	Top/sides	Wall	Outflow	Source
Pressure/ velocity	Logarithmic profile	Symmetry	Logarithmic law	Pressure	Constant velocity
Concentration	Zero	Zero	Zero normal gradient	Zero normal gradient	Constant value

roofs of the building placed with the computational domain. The computational domain measured 100H in the x-direction, 60H in the y-direction and 20H in the z-direction where H is the floor height of the buildings and has a value of 4 m.

In order to give a more realistic release of pollutant, two sources were built as shown on Fig. 3 and placed on the ground plane of the computational domain. The sources were place at 0.25 m above the ground and the CO_2 was released horizontally as would happen with vehicle exhausts. The two sources were 230 m long and were placed at the centre of 'Salem Al Mubarak St.' (see Fig. 1) between the existing Building 11 and the proposed Building 13. The length of the sources was approximately the same length as the proposed building.

After several tests for grid independence, a non-uniform Cartesian grid was used of size 300 × 200 × 120 cells in the x-, y- and z-directions respectively with refinement of the grid above building height and in the street regions. When the fluid/solid boundary intersected obliquely, some of the cells of the Cartesian grid, a technique known as PARSOL (PARtial SOLids) [37] was used to improve the accuracy of the flow simulations. A typical grid within one of the street canyons is shown on Fig. 4 with refinement in the vicinity of roofs, building walls and the ground.

Table 5 lists the calculations carried out for this work. The parameters varied were the onset wind velocity and the ambient temperature, as well as the onset wind direction. All tests were carried out first with the new building absent and then with the new building present for comparison.

The ambient temperatures were chosen to reflect the average temperatures found in Kuwait during the winter and summer months. The effect on pollutant levels of CO_2 on different values of the onset wind originating from a north-west direction was thoroughly investigated as this was considered as the worst case scenario both for pedestrians and motorists in the vicinity of 'Salem Al Mubarak St.' and for the residents of the group of residential buildings located south-east of the proposed new building.

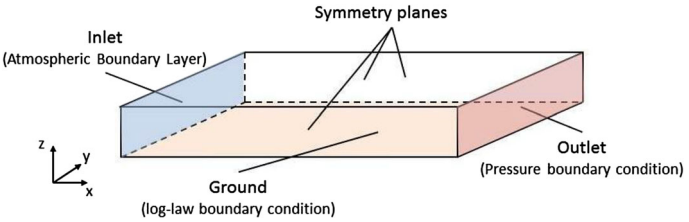

Fig. 2 Schematic showing the computational domain used

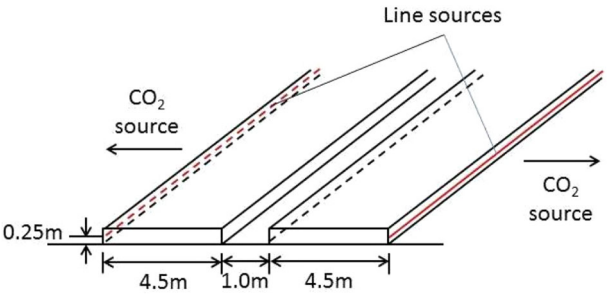

Fig. 3 Line sources used

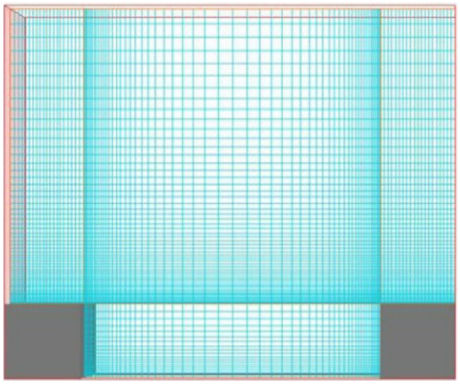

Fig. 4 Typical grid with one of the street canyons

Table 5 Calculations carried out

Test no.	Onset wind velocity (m/s)	Onset wind direction	Ambient temperature (°C)
1	0.1	From NW	25
2	4.0	From NW	25
3	6.0	From NW	25
4	0.1	From NW	50
5	4.0	From NW	50
6	6.0	From NW	50
7	0.1	From N	25
8	6.0	From N	25

4 Validation of model

The RANS model used here has already been extensively validated [23] for simple atmospheric boundary-layer flows over rough surfaces, concentrations of pollutant in 2D isolated street canyons and concentrations of pollutant in 3D urban environments against well tested and reliable experimental data bases [3, 38]. A brief summary is given here. The experimental data was obtained from a series of pollutant concentration measurements

in the atmospheric boundary layer wind tunnel at the Meteorological Institute of Hamburg University, Germany. The boundary layer was generated in a wind tunnel which consisted of an inlet nozzle, flow straighteners, Irwin-type vortex generators, a flow establishment section, a test section, anti-swirl devices and a squirrel-cage centrifugal fan. Two wooden bars were laid out across the wind tunnel to model two-dimensional multi-story flat-roofed buildings. The line source was placed in the centre of the street floor between the two bars to model the emission source from the vehicular exhaust. A mixture of air and ethane (pollutant) was ejected steadily, homogeneously and, horizontally only, from both sides of the line source at a certain flow rate.

Figure 5 shows a 3D view of the computational domain used for $B/H = 1$, where B is the street canyon width and H the building height. The actual physical domain is 0.18 m wide and 0.25 m high. The height and width of the line source are 0.0012 and 0.01 m respectively. The Cartesian grid size used was 150 in the x-direction and 100 in the z-direction. Extensive tests of grid independence were carried out with increasing grid size until further increases in grid size gave insignificant changes in calculated variable values. The grid was refined in regions of solid wall and road to capture boundary layer characteristics.

Importantly during these validation studies, it became clear that the variant RNG k–ε turbulence model used to close the equations, gave the most satisfactory results for the concentration levels in an urban environment. Typical results for calculations at the centre of a street canyon for mean velocity and turbulence kinetic energy profiles are shown on Fig. 6, where $H = 0.6$ m corresponds to the model building height used in the experimental study [38]. It can be seen that the results are satisfactory for the streamwise horizontal velocity, except near the street floor where the negative value is much larger than that measured. However, say between pedestrian and building roof level, the values calculated are in very satisfactory agreement with the experimental. The turbulent kinetic

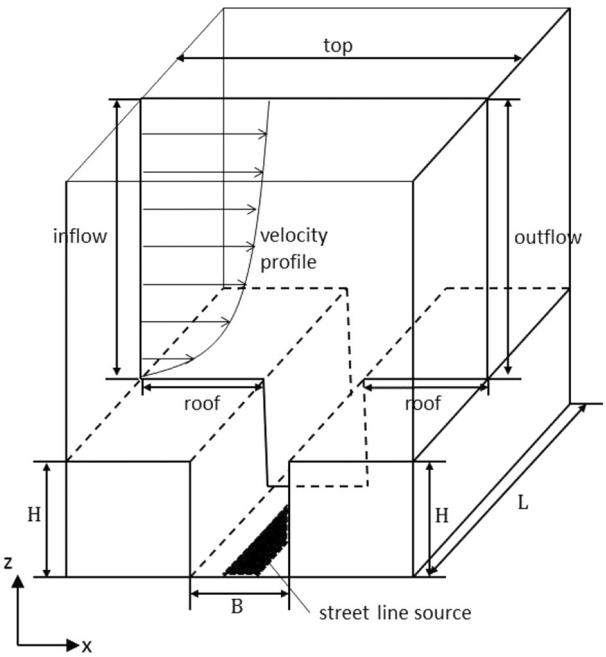

Fig. 5 Schematic diagram of the computational domain for an isolated street canyon, $B/H = 1$

energy is large near the roof level owing to strong velocity shear in this region. Except for this region over-prediction is seen along most of the profile.

Extensive validation of the computer model was also carried out for concentration levels [23]. Typical results are shown on Fig. 7, again within a street canyon for both leeward and windward sides of the street.

Here K is the dimensionless pollutant concentration given as,

$$K = \frac{CU_{ref}HL}{Q_e}, \tag{12}$$

where U_{ref} is the reference wind speed recorded at a height of 0.65 m above the street level, C is the volume fraction of the pollutant, H is the height of the building, L is the length of the line source and Q_e is the volume flow rate of the pollutant. For three turbulence models, calculations were made for the wind speeds $U_{ref} = 0.5$, 2, 4 m/s and compared with the measurements of Meroney et al. [3]. As can be seen from Fig. 7, there is considerable difference in the magnitude of K between the leeward side of the upwind building compared to windward side of the downwind building. This is reflected by both measurements and calculations. For the windward side, the pollutant concentrations are fairly constant and are small in value with the height of the downwind building, while the pollutant concentrations for the leeward side decrease in an exponential fashion from the base to the roof of the building to the roof and have a relatively large value especially close to the ground. For $U_{ref} = 0.5$ m/s, the pollutant dispersion model obtained almost identical solutions for all three turbulence models on the windward side, while for the leeward side, the standard and RNG turbulence models give very close results, whereas the realizable turbulence model provided slightly higher values. All calculations for this low reference wind speed case were in satisfactory agreement to the measurements. When the reference wind speed is increased, it can be seen that the standard and realizable k–ε turbulence models over-predict the pollutant concentrations on the leeward side and windward side of the buildings while the RNG k–ε turbulence model provides good agreement throughout for the windward side and exceptional agreement at $U_{ref} = 2$ m/s on the leeward side. However there is also a tendency for the RNG k–ε model to over predict as the reference wind speed is increased, as can be seen by the $U_{ref} = 4$ m/s case.

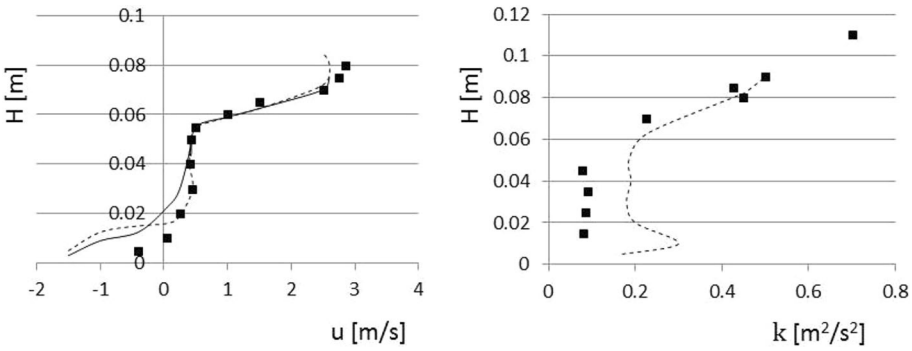

Fig. 6 Comparison of measured and calculated values of the streamwise horizontal velocity and turbulent kinetic energy at the street canyon centre with flat roofed building upstream. RNG k–ε model used. *Solid line* standard k–ε turbulence model, *dashed line* RNG k–ε turbulence model, *filled square* measured

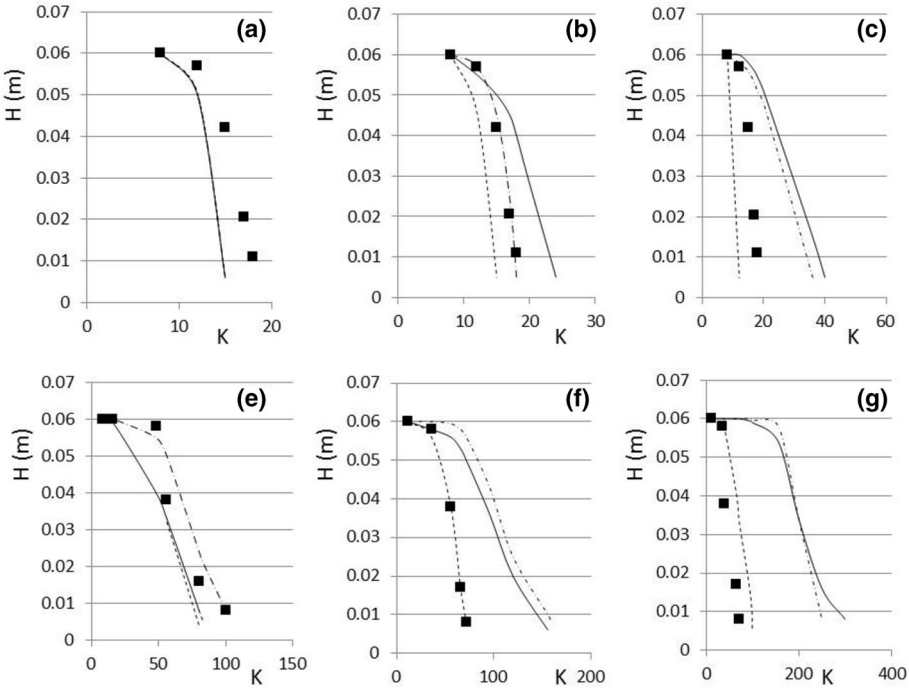

Fig. 7 Distributions of the dimensionless pollutant concentration on the windward (**a**–**c**) and leeward (**e**–**g**) sides of the buildings for different wind speeds: **a**, **e** $U_{ref} = 0.5$ m/s, **b**, **f** $U_{ref} = 2$ m/s, **c**, **g** $U_{ref} = 4$ m/s ($B/H = 1$ and $Q_e = 4$ L/h). Turbulence models: *Solid line* standard k–ε turbulence model, *dashed line* RNG k–ε turbulence model, *dashed dotted line* realizable k–ε

5 Results and discussion

Results are first shown for the mean velocity within the residential street canyon between Buildings 13 and Building 6 on Fig. 8 with the ambient temperature of 25 °C.

When the onset wind is strong, in this case 6 m/s, a well organised, rotating vortex within the canyon is noted. However for very light wind, in this case 0.1 m/s, the air flow is seen to enter and leave the canyon without rotation except for small vortices in the vicinity of the bottom corners. These mean flow patterns are significant for the transport of pollutant in that, for strong wind, any pollutant which enters the street canyon gets trapped and is resident for a relatively long time, with diffusion the main mechanism of escape. For very light wind a pollutant which enters the residential street canyon is resident for a relatively short amount of time with convection as the main means of escape. There is a notable leading-edge separation area on the roof of Building 6 generated when the wind is very light, which will also hinder the dispersion of any pollutant.

It is worth noting that when Building 13 is not present, the flow in the vicinity of the near wake of Building 11 is that of a classical backward facing step, i.e. on the upper leeward edge of Building 11 the flow separates leading to a near wake region that interacts with the development of the main horseshoe vortex wrapping around Building 11. Comparing experimental flow results [39] for Reynolds numbers based on building height (Re_H) and with the onset wind velocities of 4 and 6 m/s, the present calculated results of

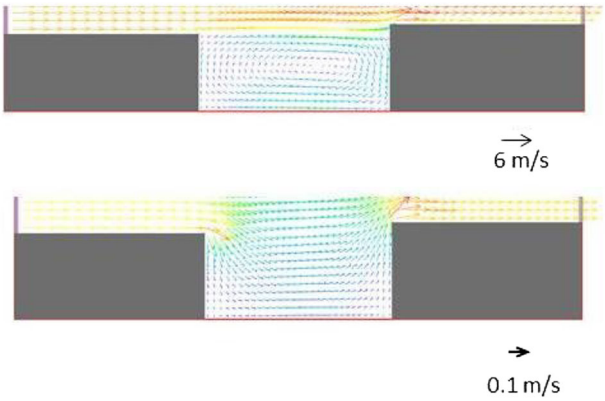

Fig. 8 Wind-speed vector distributions within the residential street between Building 13 and Building 6 for onset wind velocities of 6 and 0.1 m/s and an ambient temperature of 25 °C

$x/H \approx 1.6$ and 1.7 respectively were in good agreement. Close to the observed reattachment point a negative velocity close to the surface was computed indicating that this position is predicted to be still far inside the recirculation region, thus showing the computer model to overestimate the reattachment length. This over-prediction is a feature of the standard k–ε turbulence model [40] as well as some of its variants, and, could lead to overestimation of the transport of pollutants at a distance farther downstream than is found in reality.

5.1 Light wind

The results (plan view) for very light wind (0.1 m/s) and, an ambient temperature of 25 °C, are shown for the new building present and absent on Fig. 9. The plan view shown on Fig. 9 has been cropped for clarity with the wake flow of the buildings not shown. The calculations shown are for a height of 1.6 m from the ground. The point values included on this figure are the CO_2 pollutant values at the various locations normalized with the CO_2 pollutant values originating at the line sources, i.e. K/K_s. It can be seen the presence of the new building reduces the pollutant levels by some 33–50% and helps shield the residents and pedestrians in the residential street from severe pollution. However pedestrians and motorists on the SE side (windward side) of Salem Al Mubarak St. will suffer substantial pollutant levels whereas on the NW side (leeward side) there appears to be no rise in pollutant level.

Figure 10 give a cross-sectional view of the residential street pollution levels between Building 13 and Building 6. The pattern of pollution is in line with the velocity vectors shown on Fig. 8 and it is noticeable that the heavy CO_2 gas (some 1.67 times heavier than air) forms stratified contours.

Detailed calculations taken for the normalized CO_2 pollutant levels at the centre of the residential street are shown on Fig. 11 for very light onset wind (0.1 m/s). For such a small velocity, convergence to a solution using the residual values as the criterion can be of concern, especially, as was here, the initial velocity field guesses throughout the computational domain was set at zero. However, in the event, the residuals for all variables did attain a value less than 10^{-4}. Values are given here for Building 13 present and absent, and, for winter and summer ambient temperatures. It can be generally seen that the pollutant levels go up during the summer months but not substantially so, only reaching some 3–4%

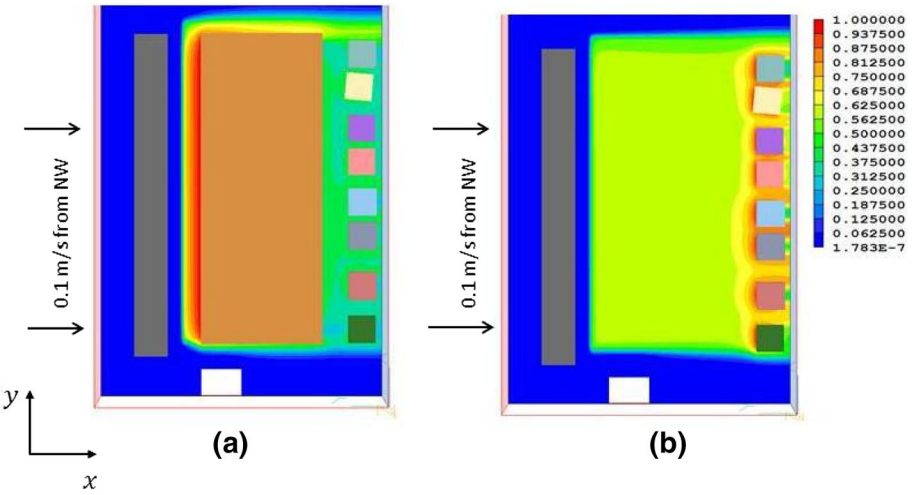

Fig. 9 Plan view of calculated pollutant levels for very light wind (0.1 m/s) for the proposed building present and absent. **a** Building 13 present, **b** Building 13 absent

higher. It is perhaps surprising that the difference between values for 25 and 50 °C were not substantially different in that the thermal mixing appears not to be as dominant as it should be. It may be that to get a more correct simulation of the pollutant levels in relation to ambient temperature, a more sophisticated modelling of heat loss at the top boundary of the computational domain may be necessary. Again the results shown are for calculations at a height of 1.6 m from the ground.

5.2 Moderate wind

Similar results were found for onset wind speeds of 4 and 6 m/s, so only the results for 4 m/s are shown on Fig. 12. Again the figures have been cropped for clarity as the

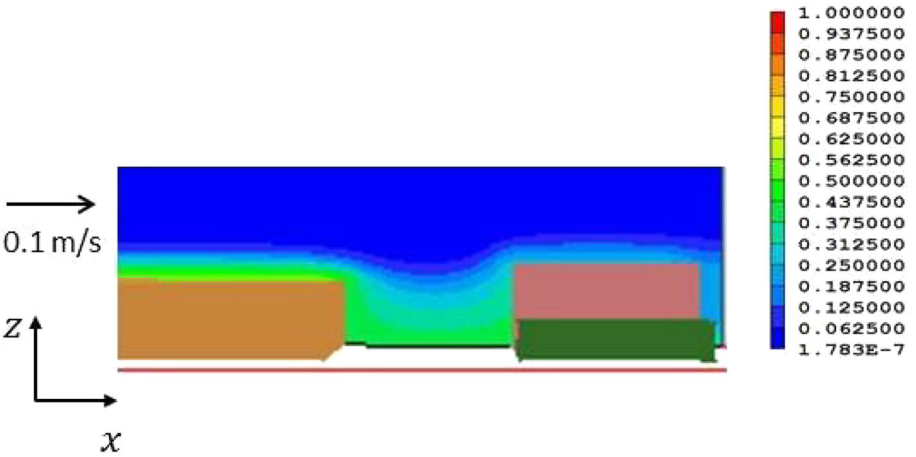

Fig. 10 Cross-sectional view of pollutant levels in residential street or very light wind

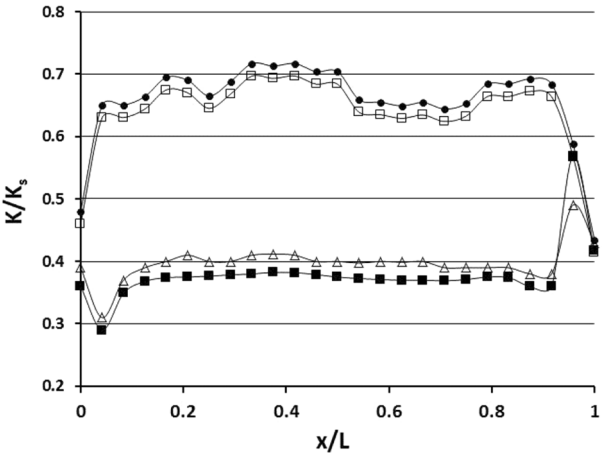

Fig. 11 CO_2 pollutant values at the centre of the residential street [between Buildings 13 and (2–9)] for very light wind, *filled square* Building 13 present 25 °C, *open triangle* Building 13 present 50 °C, *open square* Building 13 absent 25 °C, *filled circle* Building 13 absent 50 °C

computational domain used extended much further in the direction of the buildings' wake. The contours shown are for calculations at a height of 1.6 m from the ground.

The pollution patterns at these higher onset wind velocities are quite different to that generated by very light wind. There is a stronger tendency for pollutants to get trapped in Salem Al Mubarak St. with just a thin layer of pollutant travelling in the roof boundary layer of Building 13 to the residential street. There is an increase in pollutant levels on the leeward side of Building 13, but a substantial decrease in the near vicinity of the residential buildings when Building 13 is present. There is a tendency when Building 13 is not present for the pollutant to get trapped around the bases of the residential buildings. For onset wind above 8 m/s it was found that no pollutant escaped from Salem Al Mubarak St. when Building 13 was present except around the side of the building and generally no pollutant was found above 10 m no matter what the onset wind speed was.

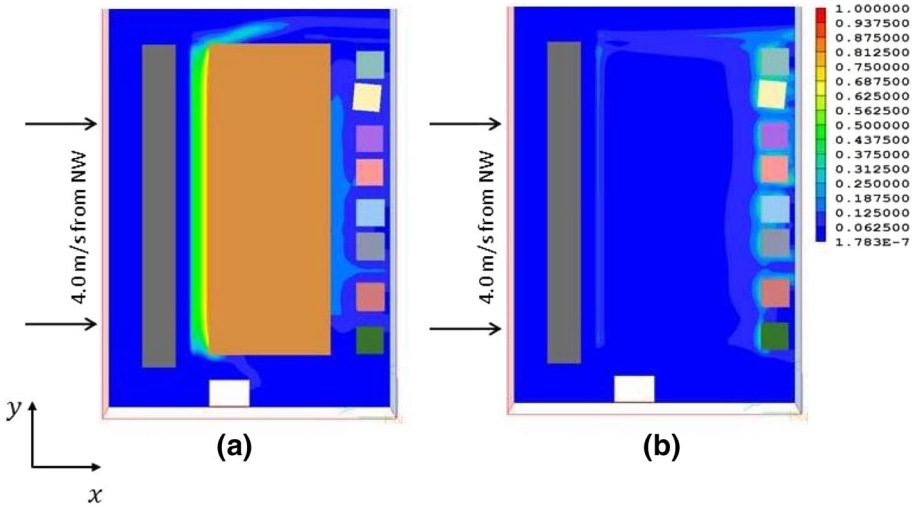

Fig. 12 Plan view of calculated pollutant levels for moderate wind (4 m/s) for the proposed building present and absent. **a** Building 13 present, **b** Building 13 absent

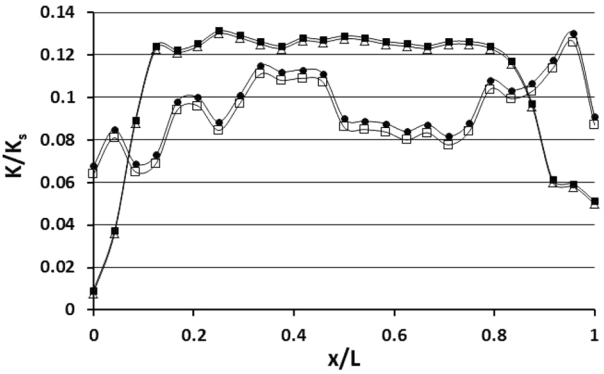

Fig. 13 CO_2 pollutant values at the centre of the residential street [between Buildings 13 and (2–9)] for very light wind, *filled square* Building 13 present 25 °C, *open triangle* Building 13 present 50 °C, *open square* Building 13 absent 25 °C, *filled circle* Building 13 absent 50 °C

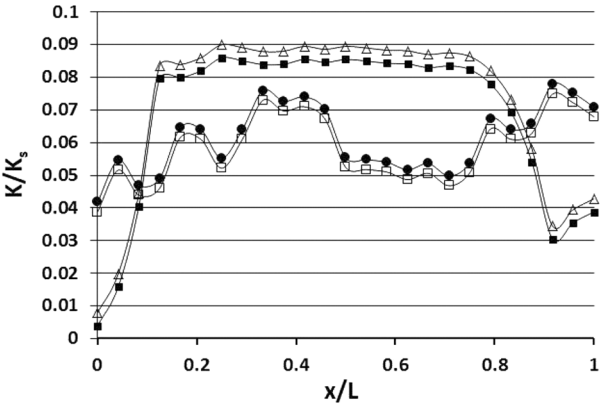

Fig. 14 CO_2 pollutant values at the centre of the residential street [between Buildings 13 and (2–9)] for very light wind, *filled square* Building 13 present 25 °C, *open triangle* Building 13 present 50 °C, *open square* Building 13 absent 25 °C, *filled circle* Building 13 absent 50 °C

Figures 13 and 14 show detailed calculations taken for the normalized CO_2 pollutant levels at the centre of the residential street for moderate wind (4 and 6 m/s respectively).

It can be seen that some pollutant is trapped in the residential street due to the presence of the new building with pollutant levels at the centre of the street going up at maximum by about 8%.

5.3 Impact of variation of wind direction

The present study was concluded by looking briefly at the impact of a variation of wind direction. Some studies were carried out with the wind coming from a northerly direction with the basic results, again calculated at a height of 1.6 metres from the ground. It can be seen from Fig. 15 that for very light wind the pollutant levels are much the same as when the wind originated from the NW but that the residential Building 10 now suffers severe pollution in addition to the pedestrians on the SE side of Salem Al Mubarak St and also in the vicinity of the NE side of the proposed new building. When the wind is moderate to strong however, as can be seen on Fig. 15 that the pollutant basically does not exist in the residential street and is eased in Salem Al Mubarak St. but again the vicinity of Building 10 sees a substantial increase in the level of pollutant.

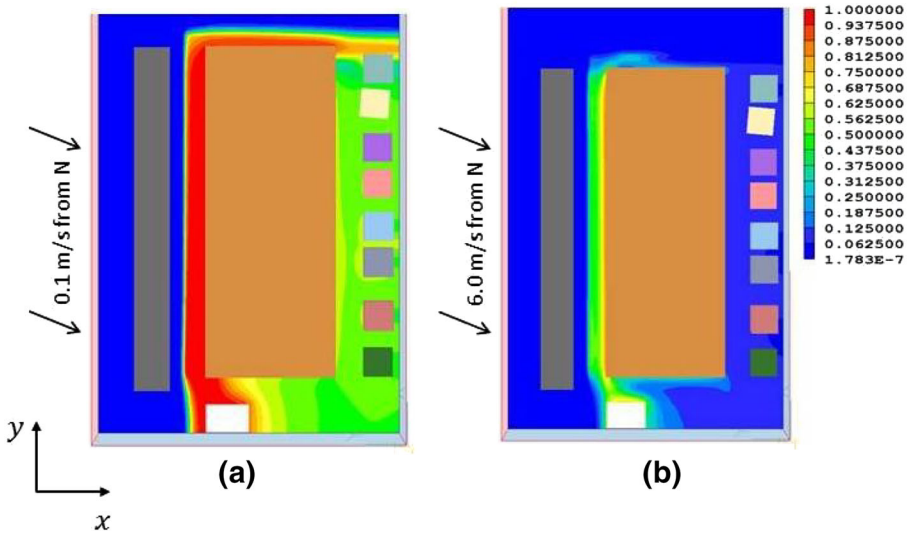

Fig. 15 Plan view of calculated pollutant levels for very light (0.1 m/s) and moderate/strong wind (6 m/s) when the wind originates from a northerly direction. **a** Building 13 present and very light wind, **b** Building 13 present and moderate/strong wind

6 Conclusions

Fairly detailed calculations have been carried in the vicinity of a proposed new shopping centre in Salmiya, Kuwait to ascertain the buildings impact on pollutant levels, namely CO_2 on the residential buildings and streets nearby.

It was found for very light winds originating from a north-western direction (the worst-case scenario), that the proposed building helped reduce the level of pollutant in the vicinity of the residential buildings. As the wind became more moderate to strong there was a tendency for pollutant to get trapped in the residential street.

When the wind is light, variation of the wind direction did reduce the pollutant level generally but not substantially. However variation of wind direction for moderate/strong wind tended to reduce pollutant levels to almost zero in the main residential street but made the level of pollutant stronger in the vicinity of Building 10.

The case presented here provides evidence that CFD modelling is a suitable approach to forecast effects of modifications to the Built Environment on air quality. Even for very low wind velocities the solver had no trouble with convergence. Regulatory authorities should make it mandatory to submit results of this approach during the building permit process in order to ensure that modifications to the Built Environment do not lead to detrimental effects on the populations' health.

Acknowledgements The authors are pleased to acknowledge the contribution of Ms. Nadya Al-Mousa, Australian College of Kuwait, in providing the drawing of the urban environment used in this study.

References

1. Longhurst JWW, Lindley SJ, Conla DE, Watson AFR (1994) Emissions of air pollutants in the north west region of England. In: Proceedings of the second international conference on air pollution II, Barcelona, Spain, vol 2, pp 99–106

2. Schatzmann M. Air pollution in German cities. In: Proceedings of the 10th world clean air conference, Helsinki, Finland, vol 2, 1995, p 222
3. Meroney RN, Pavagaeu M, Rafailidis S, Schatzmann M (1996) Study of line source characteristics for 2-D physical modelling of pollutant dispersion in street canyons. J Wind Eng Ind Aerodyn 62:37–56
4. Fenger J (1999) Urban air quality. Atmos Environ 33:4877–4900
5. Colvile RN, Hutchinson EJ, Mindell JS, Warren RF (2001) The transport sector as a source of air pollution. Atmos Environ 35:1537–1565
6. Kenessariyev U, Golub A, Brody M, Dosmukhametov A, Amrin M, Erzhanova A, Kenessary D (2013) Human health cost of air pollution in Kazakhstan. J Environ Prot 4:869–876
7. HEI (2000) Traffic-related air pollution; a critical review of the literature on emissions, exposure, and health effects. HEI Special Report 17. Health Effects Institute, Boston
8. Hildebrand WF (1999) Designing the city: towards more sustainable form. E&FN Spoon, London
9. DeCroix D, Brown M (2002) Report on CFD model evaluation using URBAN 2000 field experiment data. Technical Report, IOP 10, LA-UR-02-4755. Los Alamos National Laboratory
10. Hang J, Wang Q, Chen X, Sandbery M, Zhu W, Buccolieri R, Di Sabatino S (2015) City breathability in medium density urban-like geometries evaluated through the pollutant transport rate and the net escape velocity. Build Environ 94:166–182
11. Yuan C, Ng E, Norford LK (2014) Improving air quality in high-density cities by understanding the relationship between air pollutant dispersion and urban morphologies. Build Environ 71:245–258
12. Baik JJ, Kim YS, Kim JJ (2007) Modeling reactive pollutant dispersion in an urban street canyon. Atmos Environ 41:934–989
13. Blocken B, Stathopoulos T, Saathoff P, Wang X (2008) Numerical evaluation of pollutant dispersion in the built environment: comparisons between models and experiments. J Wind Eng Ind Aerodyn 96(10–11):1817–1831
14. Britter RE, Hanna SR (2003) Flow and dispersion in urban areas. Annu Rev Fluid Mech 35:469–496
15. Kim JJ, Baik JJ (2004) A numerical study of the effects of ambient wind direction on flow and dispersion in urban street canyons using the RNG k–ε turbulence model. Atmos Environ 38:3039–3048
16. Lien FS, Yee E (2004) Numerical modeling of the turbulent flow developing within and over a 3-D building array, part 1: a high-resolution Reynolds-averaged Navier–Stokes approach. Boundary-Layer Meteorol 112:427–466
17. Lateb M, Meroney RN (2016) On the use of numerical modelling in a near-field pollutant dispersion in urban environments—a review. Environ Pollut 208:271–283
18. Meroney RN (2016) Ten questions concerning hybrid computational/physical model simulation of wind flow in the built environment. Build Environ 96:12–21
19. Yakhot V, Orszag SA (1986) Renormalization group analysis of turbulence: I. Basic theory. J Sci Comput 1(1):1–51
20. Leitl BM, Meroney RN (1997) Car exhaust dispersion in a street canyon: numerical critique of a wind tunnel experiment. J Wind Eng Ind Aerodyn 67&68:293–304
21. Cui P-Y, Zhuo L, Wen-Quan T (2016) Buoyancy flows and pollutant dispersion through different scale urban areas: CFD simulations and wind-tunnel measurement. Build Environ 104:76–91
22. Flores F, Garreaud R, Muñoz R (2013) CFD simulations of turbulent buoyant atmospheric flows over complex geometry: solver development in OpenFOAM. Comput Fluids 82:1–13
23. Adair D, Jaeger M (2015) Reynolds-averaged Navier–Stokes modelling of air pollution at the local urban scale. Eng Appl Comput Fluid Dyn 4:119–136
24. Adair D, Jaeger M (2015) Evaluation for air pollution in the vicinity of roadside solid barriers. Energy Environ Eng 2(7):145–152
25. Zadeh FH (2014) Transport-environment case study of Hamad Al-Mubarak Corridor in Al-Salmiya Area, State of Kuwait. Thesis, Australian College of Kuwait, Department of Civil Engineering
26. Ltd Cham (2015) PHOENICS CODE 2014. Cham Ltd., Wimbledon
27. Tominaga Y, Stathopoulos T (2007) Turbulent Schmidt numbers for CFD analysis with various types of flowfield. Atmos Environ 41:8091–8099
28. Di Sabatino S, Buccolieri R, Pulvirenti B, Britter R (2007) Simulation of pollutant dispersion within idealized urban-type geometries with CFD and integral models. Atmos Environ 41(37):8316–8329
29. Hang J, Li Y, Sandberg M, Buccolieri R, Di Sabatino S (2012) The influence of building height variability on pollutant dispersion and pedestrian ventilation in idealized high-rise urban areas. Build Environ 56:346–360
30. Chavez M, Stathopoulos T, Bahloul A. CFD modelling of flow and dispersion in the built environment: different RANS models and a first attempt to use URANS. In: 7th International colloquium on bluff aerodynamics and applications, Shanghai, 2–6 Sept 2012, pp 978–988

31. Hargraves DM, Wright NG (2007) On the use of the k–ε model in commercial CFD software to model the neutral atmospheric boundary layer. J Wind Eng Ind Aerodyn 95(5):355–369
32. Di Sabatino S, Buccolieri R, Olesen HR, Ketzel M, Berkiwicz R, Franke J, Schatzmann M, Schlunzen KH, Leitl B, Britter R, Borrego C, Costa AM, Trini Castelli A, Reisin TG, Hellsten A, Saloranta J, Moussiopoulos N, Barmpas F, Brzozowski K, Goricsan I, Balczo M, Bartzis JG, Efthimiou G, Satiago JL, Martilli A, Piringer M, Baumann-Stanzer K, Hirtl M, Baklanov AA, Nuterman RB, Starchenko AV (2011) COST 732 in practice: the MUST model evaluation exercise. Int J Environ Pollut 44(1/2/3/4):403–418
33. Meroney R, Ohba R, Leitl B, Kondo H, Grawe D, Tominaga Y (2016) Review of CFD guidelines for dispersion modeling. Fluids 1(14):1–16
34. Tominaga Y, Mochida A, Yoshie R, Kataoka H, Nozu T, Yoshikawa M et al (2008) All guidelines for practical applications of CFD to pedestrian wind environment around buildings. J Wind Eng Ind Aerodyn 96:1749–1761
35. Lien FS, Leschziner MA (1994) Upstream monotonic interpolation for scaler transport with application to complex turbulent flows. Int J Numer Methods Fluids 19:527–548
36. Patankar SV (1980) Numerical heat transfer and fluid flow. Hemisphere, Washington, DC
37. Ludwig J, Mortimore S (2011) PHOENICS-VR Reference Guide. CHAM TR 326, Wimbledon
38. CEDVAL Dataset (2002) Category B1-4 (flow across an intersection). http://www.mi.uni-hamburg.de/cedval. Accessed Nov 2014
39. Durst F, Tropea C (1982) Flows over two-dimensional backward-facing steps. In: IUTAM symposium. Springer, Marseille
40. Schmidt S, Thiele F (2002) Comparison of numerical methods applied to the flow over wall mounted cubes. Int J Heat Fluid Flow 23:330–339